JOURNAL OF AIRCRAFT
Vol. 46, No. 1, January–February 2009

Development of Stable Automated Cruise Flap for an Aircraft with Adaptive Wing

Craig Cox,* Ashok Gopalarathnam,† and Charles E. Hall Jr.†
North Carolina State University, Raleigh, North Carolina 27695

DOI: 10.2514/1.38684

Cruise flaps are devices designed to minimize drag, and previous research has explored using a wing-based pressure differential to automate them. Different presentations of the pressure-differential data tend to lead to the development of different types of controllers for automated cruise flaps. A presentation used by previous researchers led to an unstable drag-minimizing controller, whereas a presentation used in this research leads to a stable controller that implements multiple functions. Techniques previously used for high Reynolds number natural-laminar-flow airfoils are modified for use with the low Reynolds number SD7037 planned for future flight testing. The results of rigid-aircraft simulations are presented, showing the effectiveness of the multifunction controller, which is able to simultaneously reduce drag and alleviate the effects of vertical gusts.

Nomenclature

C_L	=	aircraft lift coefficient
C_{L_w}	=	wing lift coefficient
C_{L_α}	=	change in aircraft lift due to angle of attack
$C_{L_{\dot\alpha}}$	=	change in aircraft lift due to the derivative of angle of attack
$C_{L_{\alpha,w}}$	=	change in wing lift due to angle of attack
$C_{L_{\delta_e}}$	=	change in aircraft lift due to elevator deflection
$C_{L_{\delta_f}}$	=	change in aircraft lift due to flap deflection
$C_{L_{\dot\delta_f}}$	=	change in aircraft lift due to derivative of flap deflection
$C_{L_{\delta_f,w}}$	=	change in wing lift due to flap deflection
C_l	=	airfoil lift coefficient
C_{m_α}	=	change in aircraft pitching moment due to angle of attack
$C_{m_{\dot\alpha}}$	=	change in aircraft pitching moment due to the derivative of angle of attack
$C_{m_{\delta_e}}$	=	change in aircraft pitching moment due to elevator deflection
$C_{m_{\delta_f}}$	=	change in aircraft pitching moment due to flap deflection
$C_{m_{\dot\delta_f}}$	=	change in aircraft pitching moment due to the derivative of flap deflection
K_D	=	derivative gain
K_I	=	integral gain
K_P	=	proportional gain
p_l	=	midchord lower-surface pressure
$p_{l,l}$	=	leading-edge lower-surface pressure
$p_{l,u}$	=	leading-edge upper-surface pressure
p_u	=	midchord upper-surface pressure
Re	=	Reynolds number
α	=	angle of attack
$\dot\alpha$	=	derivative of angle of attack
α_{0L}	=	angle of attack at which lift is zero
γ	=	temporary variable
ΔC_L	=	incremental aircraft lift coefficient
ΔC_{L_w}	=	incremental wing lift coefficient
ΔC_m	=	incremental aircraft pitching moment
$\Delta C_p'$	=	ratio of leading-edge pressure differential to midchord pressure differential
$\Delta\alpha$	=	incremental angle of attack
$\Delta\delta_e$	=	incremental elevator deflection
$\Delta\delta_f$	=	incremental flap deflection
δ_e	=	elevator deflection angle
δ_f	=	flap deflection angle
$\dot\delta_f$	=	derivative of flap deflection angle
τ_f	=	flap effectiveness parameter

Introduction

CRUISE flaps are trailing-edge flaps operated at small deflection angles for the purpose of reducing drag at offdesign conditions. The deflection of a cruise flap results in a shifting of the low-drag region (bucket) of the drag polar for an airfoil, as shown in Fig. 1. Flap deflection moves the leading-edge stagnation point, which affects the pressure distributions along the airfoil upper and lower surfaces. Figure 2 shows that for natural-laminar-flow (NLF) airfoils, there is a small region at the leading edge in which it is most desirable to locate the stagnation point [1,2]. Doing so results in favorable (or less adverse) pressure gradients over the upper and lower surfaces, even at offdesign coefficients of lift. Without the cruise flap, either the upper or lower surface would have experienced loss of laminar flow at these offdesign conditions. Thus, when scheduled correctly, a cruise flap can result in a large range of C_l values over which low C_d is achieved. For this reason, several NLF airfoils have been designed with cruise flaps [3–5]. Cruise flaps have also been successfully used on high-performance sailplanes for several decades.

A study of automated cruise flaps was performed by McAvoy and Gopalarathnam [6]. As shown in Fig. 3, four pressure sensors are used to determine the optimal flap position for the currently existing pressure distribution. The pressure differential across the two leading-edge sensors is compared with the pressure differential across the two midchord sensors. A simple controller adjusts the flap angle to maintain the desired ratio of pressure differentials, ensuring that the actual stagnation point remains within the ideal range on the leading edge.

Vosburg and Gopalarathnam [7] noted that an automated cruise flap could be controlled using the instantaneous coefficient of lift as the sole input. Such a flap, however, would be unstable by itself. From a trimmed state, if the wing were perturbed such that the coefficient of lift were increased, the flap angle would increase to move the stagnation point back to the ideal location. The larger flap

Presented as Paper 2008-206 at the 46th AIAA Aerospace Sciences Meeting and Exhibit, Reno, NV, 7–10 January 2008; received 21 May 2008; revision received 2 September 2008; accepted for publication 8 September 2008.

*Graduate Research Assistant, Department of Mechanical and Aerospace Engineering, Campus Box 7910. Student Member AIAA.

†Associate Professor, Department of Mechanical and Aerospace Engineering, Campus Box 7910. Senior Member AIAA.

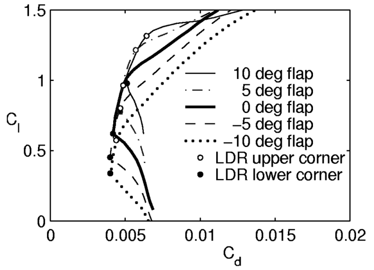

Fig. 1 Shift of low-drag region (LDR) with flap deflection.

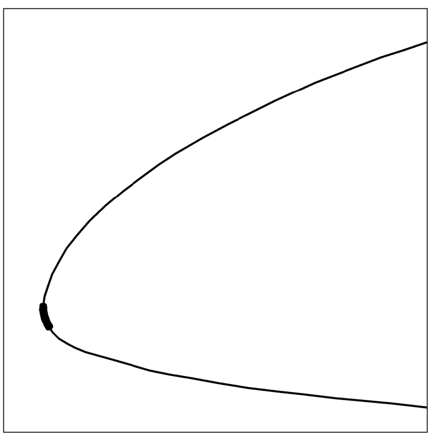

Fig. 2 Ideal stagnation-point range.

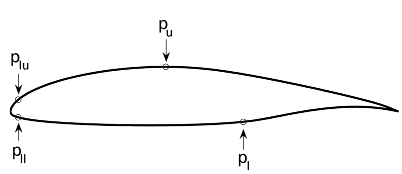

Fig. 3 Pressure port locations.

angle would then increase the coefficient of lift even more, and the flap would quickly diverge to its limit of travel. Although aircraft such as uninhabited air vehicles are probably equipped with separate autopilot control systems to maintain altitude and airspeed, such systems could not counter the instability of the flap controller, because the flap system has such a short time constant (determined primarily by the reaction time of the flap servo). A filter is needed to slow the operation of the flap.

Cox et al. [8] performed a dynamic stability analysis of the Vosburg and Gopalarathnam [7] controller to show its behavior under different operating conditions and with different filters. They also developed an aircraft controller to maintain a desired coefficient of lift using flap deflections. This type of controller is useful with segmented flaps for tailoring the spanwise lift distribution to minimize induced drag or wing-root bending moment.

Analysis of Previous Control Scheme

The ratio of leading-edge pressure differential to midchord differential is given by the following equation:

$$\Delta C_p' = \frac{p_{l,u} - p_{l,l}}{|p_u - p_l|} \tag{1}$$

For NLF airfoils with a range of flap deflections, a target $\Delta C_p'$ can be selected. If the airfoil is operated at or near this target, it is guaranteed to be operating in the low-drag region, regardless of flap angle or lift coefficient. Operations at other than the target $\Delta C_p'$ result in an error, either negative (actual $\Delta C_p'$ is too low) or positive. Assuming a negative error, there are two obvious choices: increase or decrease flap deflection. The choice of presentation of the $\Delta C_p'$ data for different flap angles affects the controllers that are developed.

The paper by McAvoy and Gopalarathnam [6] included figures similar to Fig. 4, which shows $\Delta C_p'$ as a function of C_l on the horizontal axis for the NASA NLF(1)-0215F airfoil [4]. Because the target $\Delta C_p'$ values for all flap values are close to −0.37, this value is chosen as the target value that a controller must try to maintain. Assume that an airfoil is operating in steady-state conditions at location A. There is no $\Delta C_p'$ error and so the flap does not move. A gust occurs such that C_l increases by about 0.2. Because the flap has not yet changed, the operating condition moves along the −8 deg flap curve to location B. This changes $\Delta C_p'$ from −0.37 to about −1.25, resulting in a negative error. This particular presentation of the $\Delta C_p'$ data makes it appear that the correct response is to increase flap to move along the constant C_l line to location C. Here the flap value is −2 deg and $\Delta C_p'$ returns to the optimal value of −0.37. This presentation of the $\Delta C_p'$ data tends to lead to the development of the following rule: *To fix a nonoptimal condition, determine the optimal flap value for the current C_l and move the flap toward that value.* From Fig. 4, this implies that correction of a negative $\Delta C_p'$ error requires that the flap be increased, and so there is a negative correlation between $\Delta C_p'$ error and corrective flap movement.

The paper by Vosburg and Gopalarathnam [7] included a figure similar to Fig. 5. It was used to demonstrate why a flap controller based on the preceding rule is unstable. Points A, B, and C correspond to the same points in Fig. 4. An airfoil in steady-state conditions at point A experiences a gust that increases C_l by 0.2. The operating condition moves along the −8 deg flap curve to point B, which has a C_l of about 0.65. This condition is not optimal, and so the controller determines the optimal flap angle for a C_l of 0.65 to be

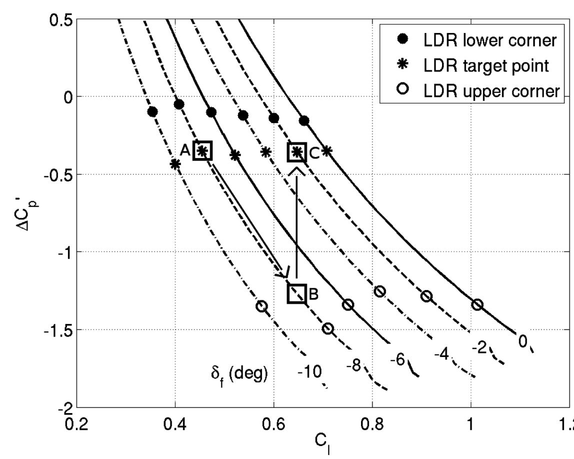

Fig. 4 Relationship between C_l and $\Delta C_p'$ for different flap angles.

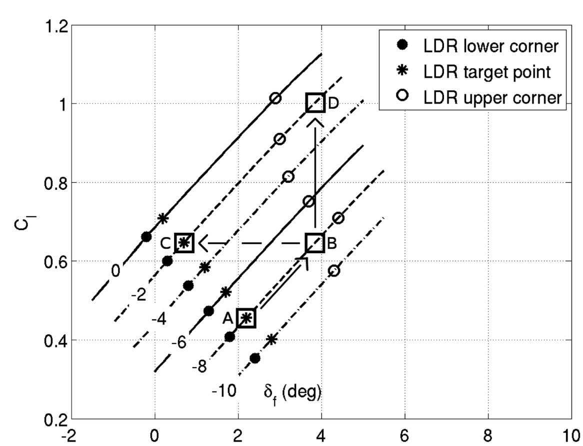

Fig. 5 Lift curves for different flap angles illustrating the behavior of an unstable flap controller.

−2 deg. The flap is increased from −8 to −2 deg, but this change does not occur along a constant-C_l line as expected, because a change in flap angle results in a change in airfoil lift. Assuming that the flap can actuate faster than the angle of attack can change, the operating condition moves along a line of constant alpha. The curves in Fig. 4 make it appear that the transition from location B will be to location C, but Fig. 5 makes it clear that the transition will instead be to location D. The optimality of location D is even worse than that of location B and in the same direction, and so the flap is unstable and will quickly diverge to its upper limit.

For such a controller to be useful, the flap cannot be fast-acting. Its response must be slow enough that as the flap is changed, the angle of attack can be changed to keep C_l constant. For an airplane, the response of the flap controller must be slower than the response of the aircraft to elevator. The controller can be slowed by passing either its input ($\Delta C_p'$) or output (commanded flap angle) through a low-pass filter. Use of such a filter (or any other slowing mechanism) makes this controller unsuitable for purposes in which a fast-acting flap is desired, such as gust alleviation.

When presenting $\Delta C_p'$ data for different flap angles, using C_l as the horizontal axis makes it easy to answer the question of what flap angle is required to achieve a target $\Delta C_p'$ for the current C_l. This question, in turn, tends to lead to the development of an unstable controller that is unsuitable for use when a fast-acting flap is desired. But there is at least one other presentation of the data that answers another question and leads to a stable controller.

The important information that Fig. 4 provides is that there is a target $\Delta C_p'$ of approximately −0.37 at which the airfoil will operate in the low-drag region. This is true regardless of the flap angle in the region of interest from about −10 to 0 deg. By using C_l as the horizontal axis, Fig. 4 makes it clear that this is also true regardless of C_l in the region of interest from about 0.35 to 0.65. Because it is true regardless of C_l, it must also be true regardless of angle of attack in an appropriate region of interest. This is made clear in Fig. 6, which presents the $\Delta C_p'$ data with α as the horizontal axis. As required, the target $\Delta C_p'$ values shown in this figure are also approximately −0.37, and so this is the value that a controller must attempt to maintain.

Assume that an airfoil is operating in steady-state conditions at location C. Points A and C correspond to the same points in Figs. 4 and 5. A gust occurs such that α increases by about 1.5 deg. Because flap has not yet changed, the operating condition moves along the −2 deg flap curve to location E. This changes $\Delta C_p'$ from −0.37 to about −1.0, resulting in a negative error. In this presentation of the $\Delta C_p'$ data it appears that the correct response is to decrease flap to move along the constant-α line to location A. Here, the flap value is −8 deg and $\Delta C_p'$ is again the optimal value of −0.37. This presentation of the $\Delta C_p'$ data tends to lead to development of the following rule: *To fix a nonoptimal condition, determine the optimal flap value for the current* α *and move the flap toward that value.* From Fig. 6, this implies that correction of a negative $\Delta C_p'$ error requires

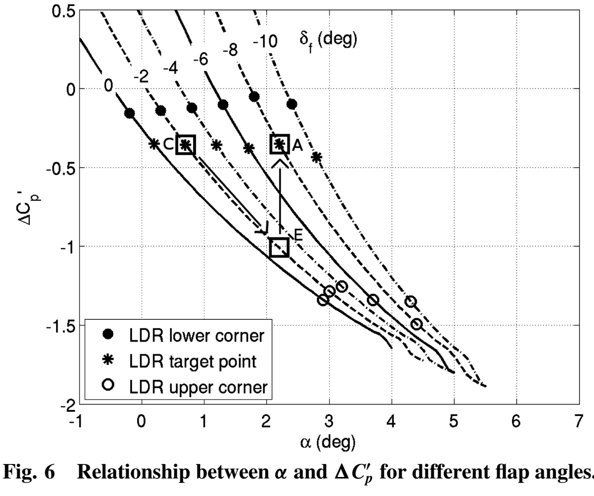

Fig. 6 Relationship between α and $\Delta C_p'$ for different flap angles.

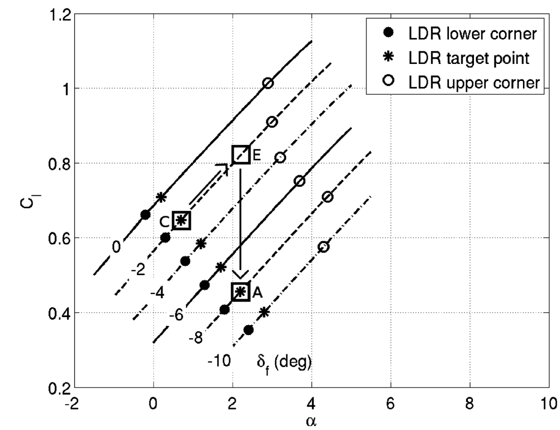

Fig. 7 Lift curves for different flap angles illustrating the behavior of a stable flap controller.

that the flap be decreased, and so there is a positive correlation between $\Delta C_p'$ error and corrective flap movement.

A flap controller based on this rule (with a positive error/correction correlation) is stable, as shown in Fig. 7. An airfoil in steady-state conditions at point C experiences a gust that increases α by 1.5 deg. The operating condition moves along the −2 deg flap curve to point E. This condition is not optimal, and so the controller determines the optimal flap angle for an α of about 2.2 deg to be −8 deg. The flap is decreased from −2 to −8 deg, and this change occurs along a constant-α line, because the flap is assumed to actuate faster than the angle of attack can change. Thus, the operating condition transitions from point E to point A, as was previously indicated in Fig. 6. The new location A is optimal, and so there is no further flap change and the controller is stable. Two equally valid presentations of the $\Delta C_p'$ data steer the development of different controllers. Figure 4 leads to a thought process that results in an unstable controller that requires a slowing filter; Fig. 6 results in a stable fast-acting controller that can also be used for purposes such as gust alleviation.

It should be noted that the simple controller illustrated in Fig. 7 is not appropriate for use without modification. After C_l, α, and $\Delta C_p'$ are perturbed by a gust, the stable response restoring the target $\Delta C_p'$ results in an overshoot of the original C_l. The final value of C_l is lower than the original, even though the effect of the gust was to increase C_l. Nevertheless, this simple controller points the way toward the development of a multifunction controller for cruise-flap automation. The advantages of three different controllers are combined to result in a cruise-flap controller with three functions: gust alleviation, $\Delta C_p'$ optimization, and $\Delta C_p'$ maintenance. The gust-alleviation function is fast-acting and uses a positive error/correction correlation to maintain current C_l. The $\Delta C_p'$ optimization function is slow-acting and uses a negative error/correction correlation to drive $\Delta C_p'$ to a target value that decreases drag. The $\Delta C_p'$ maintenance function is fast-acting and uses flap/elevator mixing to maintain current $\Delta C_p'$ in the presence of pilot input from the stick or yoke.

Simulation Model

A Simulink model was created using the AeroSim Blockset [9] from Unmanned Dynamics, LLC. The aircraft modeled is the one expected to be flight-tested in the near future: the Spirit 100 radio control (R/C) sailplane [10] from Great Planes Model Manufacturing Company. Figure 8 shows a 3-D and planform view of the lifting surfaces of the aircraft. The geometry of these surfaces was entered into Athena Vortex Lattice [11] (AVL), and stability derivatives for the aircraft were obtained from the program.

AeroSim Blockset includes a script used to determine trim values for Simulink models of powered aircraft. This script was modified for use with gliders such as the Spirit 100. References to throttle and engine speed were removed, and the ability to specify a constant descent rate was added. The modified script was used to determine

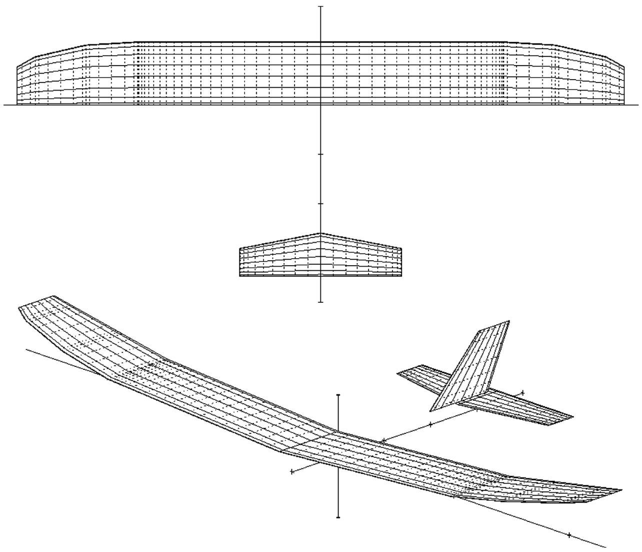

Fig. 8 AVL model of the Spirit 100 sailplane.

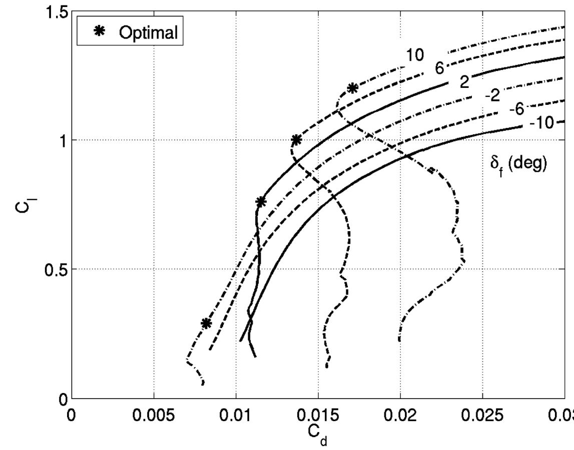

Fig. 9 SD7037 drag polars with optimal C_l values.

trim values for a number of different descent rates from 0.36 to 0.70 m/s. These descent rates correspond to trim C_L values from 1.04 to 0.40. All simulations described in this paper were performed using the case in which the trim descent rate and C_L are 0.40 m/s and 0.78, respectively.

The stability derivatives obtained from AVL include terms for δ_f, but not terms for $\dot{\delta}_f$. Because the controller to be developed will activate the flap very quickly for gust alleviation, it was determined that $\dot{\delta}_f$ derivatives should be implemented in the model. In theory, the effect of $\dot{\delta}_f$ on aircraft lift and pitching moment should be proportional to the effect of $\dot{\alpha}$. Because the effect of flap is to change the airfoil angle at which zero lift is produced (α_{0L}), the aircraft should not be able to distinguish between effects due to $\dot{\alpha}$ and those due to $\dot{\delta}_f$. The ratio of change in α_{0L} to change in δ_f is the flap effectiveness parameter τ_f, and so the following are the calculated $\dot{\delta}_f$ derivatives:

$$C_{L_{\dot{\delta}_f}} = C_{L_{\dot{\alpha}}}\tau_f \tag{2a}$$

$$C_{m_{\dot{\delta}_f}} = C_{m_{\dot{\alpha}}}\tau_f \tag{2b}$$

Earlier research regarding $\Delta C_p'$ was performed using NLF airfoils at fairly high Reynolds numbers. Drag polars at high Reynolds numbers are well-behaved with predictable flap-induced changes. It was with reduced Reynolds numbers $Re\sqrt{C_l}$ between 6×10^6 and 10×10^6, for example, that McAvoy and Gopalarathnam [6] first discovered that constant-$\Delta C_p'$ operations occur in the drag bucket for the NLF(1)-0215F and NLF(1)-0414F airfoils. Drag polars in the Reynolds number ranges corresponding to R/C aircraft, however, are much less well-behaved with respect to constant-$\Delta C_p'$ operations.

The Spirit 100 uses the SD7037 airfoil [12] designed for efficiency at low Reynolds numbers. As such, its drag polars are affected by phenomena that are not normally significant at higher Reynolds numbers. Figure 9 shows the drag polars for flap angles from −10 to 10 deg at a reduced Reynolds number of 123,000. Asterisks mark the optimal C_l values for each flap from −2 to 10 deg. Note that this optimal value is not the C_l at which the airfoil with a certain flap angle has minimum drag. That criteria for optimality would indicate which C_l should be used for a specified flap angle. What is needed, however, is the required flap angle for a specified C_l. The aircraft should operate on the Pareto front of all drag polars, which is different from the set of minimum drag positions for each polar. The optimal point for each flap angle is the midpoint of the range of C_l values for which the flap is optimal. For example, a 4 deg flap deflection (not shown) is optimal for C_l values from 0.83 to 0.95. Below 0.83, a 2 deg flap deflection is better, and above 0.95, a 6 deg deflection is better. So the optimal value for a 4 deg deflection is selected as the midpoint of 0.89. This method of determining optimality is better for the purpose of drag minimization.

For the high Reynolds number NLF airfoils used in previous research, optimal flap angles resulted in $\Delta C_p'$ values that were essentially constant. This is not the case for the low Reynolds number SD7037 airfoil. The asterisks in Fig. 10 correspond to those in Fig. 9 (i.e., they indicate the optimal C_l value for each flap). The $\Delta C_p'$ values are spread over a range of almost 6 (from −2.1 for the 10 deg flap curve to 3.7 for the 4 deg flap curve, which is not shown). For the NLF airfoil, this range was about 0.1 (from −0.45 to −0.35). The large spread for the low Reynolds number airfoil means that any constant-$\Delta C_p'$ controller developed will not be able to optimally minimize drag over all C_l values. However, by careful selection of a constant-target-$\Delta C_p'$ value, the controller can still decrease drag (nonoptimally) over some useful range of C_l values. Also, this research is expected to progress toward higher Reynolds number applications in which a constant $\Delta C_p'$ does minimize drag over reasonable values of C_l. Finally, once the behavior of a constant-$\Delta C_p'$ controller is understood, a variable-$\Delta C_p'$ controller can more easily be developed (if necessary) to minimize drag for low Reynolds number applications.

A number of trial $\Delta C_p'$ targets were tested to determine the effect of each on the drag polars. It was desired to have close to minimum drag near a C_l of 0.78, which is the trim C_l for the Spirit 100 descending at 0.4 m/s. A $\Delta C_p'$ of −1.85 was selected as the target that the controller would hold constant for purposes of drag minimization. Figure 11 shows the data of Fig. 10, with asterisks indicating the target $\Delta C_p'$ value of −1.85 for each flap value.

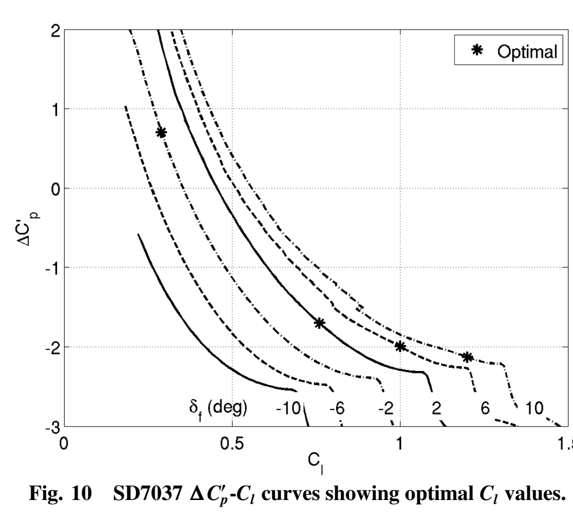

Fig. 10 SD7037 $\Delta C_p'$-C_l curves showing optimal C_l values.

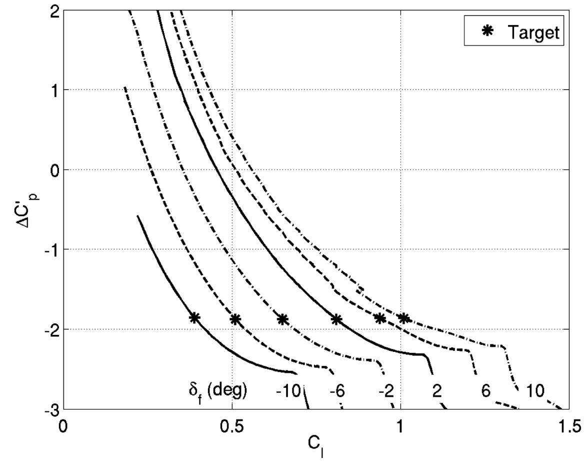

Fig. 11 Constant $\Delta C'_p$ value of −1.85 for the SD7037.

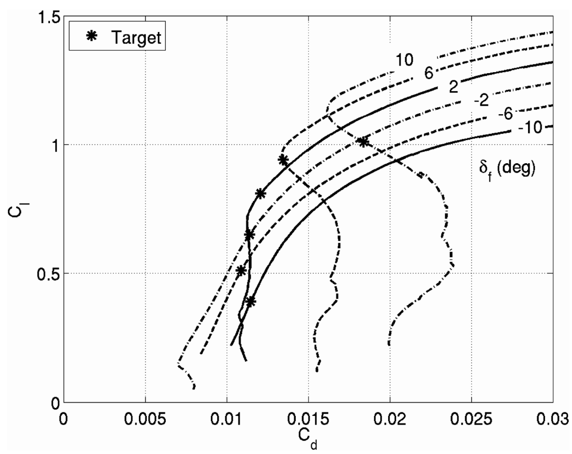

Fig. 12 Drag polars for a $\Delta C'_p$ target of −1.85 for the SD7037.

Figure 12 shows the locations of the constant-$\Delta C'_p$ targets on the drag polars. The target for a 2 deg flap deflection is near optimal around a C_l of 0.8. Most other targets are not far from optimal, but the drag penalty is fairly large at C_l values above 0.9 or below 0.5. Moving the $\Delta C'_p$ target slightly around −1.85 did not have much effect on drag around the trim lift value of 0.78, but it had large adverse effects at the flap (and C_l) extremes.

Coefficient Determination

There are a number of coefficients that must be determined for use in the controller. The value of $\Delta C'_p$ is determined from wing lift, and so several coefficients are calculated using it instead of aircraft lift. Wing lift is dependent on angle of attack and flap only and does not include tail downwash effects. For the purpose of controller development, it is not actual wing lift, but incremental wing lift, that is important:

$$\Delta C_{L_w} = C_{L_{\alpha,w}} \Delta\alpha + C_{L_{\delta_f,w}} \Delta\delta_f \tag{3a}$$

$$= C_{L_{\alpha,w}} \Delta\alpha + C_{L_{\alpha,w}} \tau_f \Delta\delta_f \tag{3b}$$

Because the controller must respond to pilot requests from the stick or yoke, it is necessary to know how trim wing lift will be affected for a given elevator deflection (and no flap deflection). Lift and pitching moment equations are manipulated to produce the desired coefficient:

$$\Delta C_{L_w} = C_{L_{\alpha,w}} \Delta\alpha \tag{4a}$$

$$0 = \Delta C_m = C_{m_\alpha} \Delta\alpha + C_{m_{\delta_e}} \Delta\delta_e \tag{4b}$$

$$\left(\frac{\mathrm{d}C_{L_w}}{\mathrm{d}\delta_e}\right)_{C_m=0} = \frac{-C_{L_{\alpha,w}} C_{m_{\delta_e}}}{C_{m_\alpha}} \tag{4c}$$

The following coefficient is presented without explanation because its derivation is similar to the preceding, except for the use of aircraft lift instead of wing lift:

$$\left(\frac{\mathrm{d}C_L}{\mathrm{d}\delta_e}\right)_{C_m=0} = C_{L_{\delta_e}} - \frac{C_{L_\alpha} C_{m_{\delta_e}}}{C_{m_\alpha}} \tag{5}$$

One of the controller functions will involve moving the flap and elevator together such that the trim wing lift does not change. It is necessary to know the elevator-to-flap mixing ratio that results in no change of trim wing lift. Lift and pitching moment equations are manipulated to produce the desired coefficient:

$$0 = \Delta C_{L_w} = C_{L_{\alpha,w}} \Delta\alpha + C_{L_{\delta_f,w}} \Delta\delta_f \tag{6a}$$

$$0 = \Delta C_m = C_{m_\alpha} \Delta\alpha + C_{m_{\delta_f}} \Delta\delta_f + C_{m_{\delta_e}} \Delta\delta_e \tag{6b}$$

$$\left(\frac{\mathrm{d}\delta_e}{\mathrm{d}\delta_f}\right)_{C_{L_w}=\mathrm{const}} = \frac{C_{m_\alpha} C_{L_{\delta_f,w}} - C_{L_{\alpha,w}} C_{m_{\delta_f}}}{C_{L_{\alpha,w}} C_{m_{\delta_e}}} \tag{6c}$$

There are other necessary coefficients that depend on $\Delta C'_p$. These coefficients require analysis of the $\Delta C'_p$ data obtained from an airfoil analysis code such as XFOIL [13]. Because the XFOIL data are highly nonlinear at the flap extremities, these coefficients rely on linear fits of data over smaller ranges of flap values. These smaller ranges are selected such that the data in question are fairly linear and always include the operating condition about which the aircraft is trimmed.

It is necessary to know how much flap is required to change $\Delta C'_p$ at a constant wing lift. The wing lift at which this value will be calculated is the trim wing lift coefficient of 0.78. Figure 11 shows C_L and δ_f values for a range of flap deflections. Figure 13 shows the result of taking a vertical slice of the data at the trim wing C_L of 0.78. The data for flap values below −2 or above 6 deg are nonlinear and are rejected. A linear fit of the remaining data produces the following coefficient:

$$\left(\frac{\mathrm{d}\delta_f}{\mathrm{d}\Delta C'_p}\right)_{C_{L_w}=\mathrm{const}} = 0.1562 \text{ rad}$$

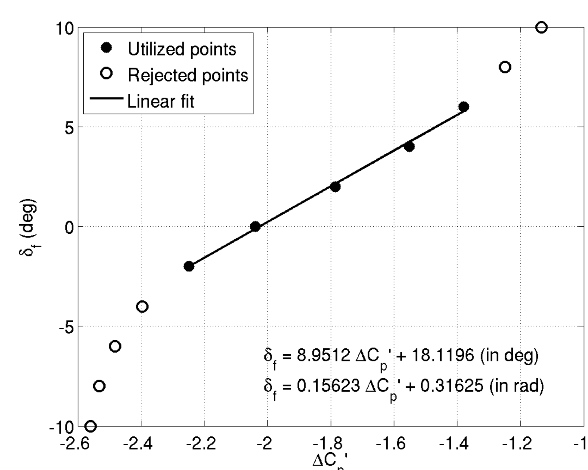

Fig. 13 Linear fit of $\Delta C'_p$-δ_f data for a wing lift coefficient of 0.78.

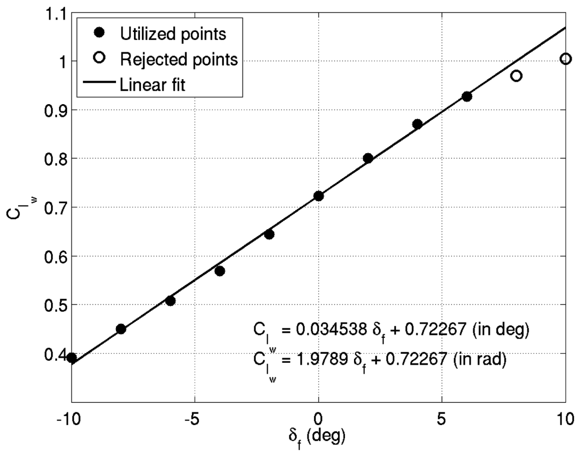

Fig. 14 Linear fit of δ_f-C_{l_w} data for $\Delta C_p'$ of 1.85.

Another value that can be extracted from Fig. 11 is the amount of wing lift change due to flap deflection when $\Delta C_p'$ is held constant. Figure 14 shows the result of taking a horizontal slice of the data at the target $\Delta C_p'$ of -1.85. The data for flap values above 6 deg are nonlinear and are rejected. A linear fit of the remaining data produces the following coefficient:

$$\left(\frac{\mathrm{d}C_{L_w}}{\mathrm{d}\delta_f}\right)_{\Delta C_p'=\mathrm{const}} = 1.9789/\mathrm{rad}$$

There are two final coefficients that are needed for the controller. For a given desired change in aircraft C_L, how should the flap and elevator be deflected so that $\Delta C_p'$ remains constant? The following equations are used:

$$\Delta C_L = C_{L_\alpha}\Delta\alpha + C_{L_{\delta_e}}\Delta\delta_e + C_{L_{\delta_f}}\Delta\delta_f \tag{7a}$$

$$0 = \Delta C_m = C_{m_\alpha}\Delta\alpha + C_{m_{\delta_e}}\Delta\delta_e + C_{m_{\delta_f}}\Delta\delta_f \tag{7b}$$

$$\Delta C_{L_w} = C_{L_{\alpha,w}}\Delta\alpha + C_{L_{\alpha,w}}\tau_f\Delta\delta_f \tag{7c}$$

$$\Delta C_{L_w} = \left(\left(\frac{\mathrm{d}C_{L_w}}{\mathrm{d}\delta_f}\right)_{\Delta C_p'=\mathrm{const}}\right)\Delta\delta_f \tag{7d}$$

Equation (7d) enforces the requirement that as the flap changes, the wing lift coefficient must change such that $\Delta C_p'$ is held constant. Combining Eqs. (7c) and (7d) produces the following:

$$\Delta\alpha = \gamma\Delta\delta_{f'} \tag{7e}$$

where

$$\gamma = \frac{(\mathrm{d}C_{L_w}/\mathrm{d}\delta_f)_{\Delta C_p'=\mathrm{const}}}{C_{L_{\alpha,w}}} - \tau_f$$

Substituting Eq. (7e) into Eqs. (7a) and (7b) produces equations for the following coefficients:

$$\left(\frac{\mathrm{d}\delta_f}{\mathrm{d}C_L}\right)_{\Delta C_p'=\mathrm{const}} = \frac{C_{m_{\delta_e}}}{C_{m_{\delta_e}}(C_{L_\alpha}\gamma + C_{L_{\delta_f}}) - C_{L_{\delta_e}}(C_{m_\alpha}\gamma + C_{m_{\delta_f}})} \tag{7f}$$

$$\left(\frac{\mathrm{d}\delta_e}{\mathrm{d}C_L}\right)_{\Delta C_p'=\mathrm{const}} = \frac{-(C_{m_\alpha}\gamma + C_{m_{\delta_f}})}{C_{m_{\delta_e}}(C_{L_\alpha}\gamma + C_{L_{\delta_f}}) - C_{L_{\delta_e}}(C_{m_\alpha}\gamma + C_{m_{\delta_f}})} \tag{7g}$$

This provides the final coefficients needed to design and implement the controller.

Controller Functions

The controller has three functions that can be activated independently. The first is gust alleviation. Because the current flap angle and $\Delta C_p'$ are available at all times, the instantaneous wing lift can be determined using the data in Fig. 11. If the aircraft enters an area of increased updraft, this will increase the angle of attack and thus the lift produced by the wing. As the aircraft flies out of the updraft, the angle of attack and wing lift will decrease. By sending the wing lift through a high-pass filter, lower-frequency semisteady lift values are removed and the resulting signal contains only the higher-frequency gust effects. The gust-alleviation function uses this signal as an error and thus attempts to minimize the effects. Figure 15 shows a portion of the model for the gust-alleviation function. The error signal is amplified by a proportional gain of 9 to make the flap more effective in reducing the error. This gain value could theoretically reduce the error by 90%, but delays introduced by the flap servo cause the reduction to be less effective. The amplified signal is multiplied by the inverse of $-C_{L_{\delta_{f,w}}}$ to determine how much flap is required to offset the wing lift error.

The second controller function is $\Delta C_p'$ optimization. If the aircraft is operating at a $\Delta C_p'$ value other than the target of -1.85, the flap and elevator should be adjusted to bring $\Delta C_p'$ back to the target value without changing the wing lift coefficient. Unlike gust alleviation, which requires a fast-acting flap, $\Delta C_p'$ optimization occurs over a period of several seconds or even tens of seconds. In smooth-air cruising conditions, this delay is insignificant because wing lift changes very slowly. In gusty conditions, $\Delta C_p'$ will vary rapidly as wing lift changes. The $\Delta C_p'$ optimization will slowly adjust the flap and elevator such that the time-averaged value of $\Delta C_p'$ is at or near the target value of -1.85. Rapid use of the flap to quickly optimize $\Delta C_p'$ would conflict with the gust-alleviation function. For example, an updraft would cause the flap to decrease for gust alleviation but increase for $\Delta C_p'$ optimization; that is why gust alleviation uses a high-pass filter to ignore low-frequency (steady-state) inputs and $\Delta C_p'$ optimization uses a low-pass filter to ignore high-frequency (transient) inputs.

Figure 16 shows the model for the $\Delta C_p'$ optimization function. The target $\Delta C_p'$ of -1.85 is subtracted from the actual value to determine the error. A low-pass filter with a time constant of 20 s removes transients from the error. This filtered error is passed through a PID (proportional–integral–derivative) controller with gains $K_P = 3.84$, $K_I = 0.192$, and $K_D = 1.28$ to improve dynamic response and eliminate steady-state error. The controller output is multiplied by $-(\mathrm{d}\delta_f/\mathrm{d}\Delta C_p')_{C_{L_w}=\mathrm{const}}$ to determine how much flap is needed to correct the $\Delta C_p'$ error without changing trim wing lift. The resulting flap command is multiplied by $(\mathrm{d}\delta_e/\mathrm{d}\delta_f)_{C_{L_w}=\mathrm{const}}$ to determine how much elevator is required to offset the flap deflection so that trim wing lift does not change. Regardless of what is needed to

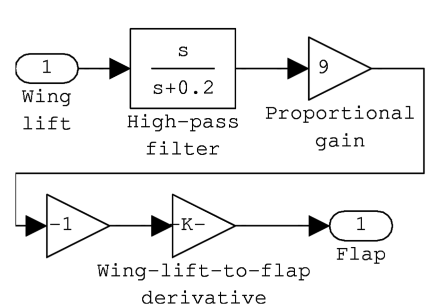

Fig. 15 Partial block diagram of the gust-alleviation function.

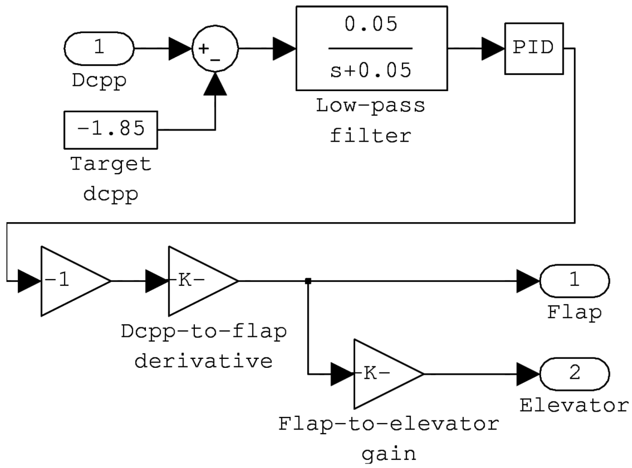

Fig. 16 Block diagram of the $\Delta C_p'$ optimization function.

optimize $\Delta C_p'$, this function always mixes flap and elevator commands such that trim wing lift does not change.

The third controller function is $\Delta C_p'$ maintenance. In an aircraft without automated cruise flaps, an elevator deflection causes the aircraft to move from one trim lift coefficient to another. For a given amount of elevator deflection commanded by the pilot, the change in trim lift coefficient can be determined. This lift change will cause steady-state $\Delta C_p'$ to change because it is accomplished without any change in the flap. If the desired lift change is to be accomplished without changing steady-state $\Delta C_p'$, the flap must be deflected as well. This is the purpose of $\Delta C_p'$ maintenance. When the pilot provides an elevator input, the controller moves the flap and elevator in a manner such that the desired lift change is provided, but steady-state $\Delta C_p'$ does not change (i.e., it is maintained).

There are two differences between $\Delta C_p'$ maintenance and $\Delta C_p'$ optimization. First, optimization strives to move $\Delta C_p'$ to the target value of -1.85 while keeping wing lift constant. Maintenance strives to keep $\Delta C_p'$ constant while providing an aircraft lift change requested by the pilot. If the original $\Delta C_p'$ is something other than the target of -1.85, maintenance attempts to maintain the original value and does not try to move it to -1.85. Second, optimization is concerned with the low-frequency (steadier) $\Delta C_p'$ error and thus activates the flap and elevator slowly in response to a time-averaged signal. Maintenance is concerned with instantaneous pilot input from the stick or yoke and activates the flap and elevator immediately. There is no low-pass filter in the maintenance function to slow flap and elevator motion.

Figure 17 shows the model for the $\Delta C_p'$ maintenance function. A pilot request from the stick or yoke is multiplied by $(\mathrm{d}C_L/\mathrm{d}\delta_e)_{C_m=0}$ to determine the change in trim aircraft lift that would occur at the requested elevator angle. This lift change is then multiplied by $(\mathrm{d}\delta_f/\mathrm{d}C_L)_{\Delta C_p'=\mathrm{const}}$ and $(\mathrm{d}\delta_e/\mathrm{d}C_L)_{\Delta C_p'=\mathrm{const}}$ to determine the flap and elevator angles that will provide the requested lift change without changing $\Delta C_p'$.

The issue of interference between the three functions must be addressed. An analysis of frequency responses is useful to determine where there may be problems. The gust-alleviation function uses a high-pass filter with a time constant of 5, and so its frequency domain

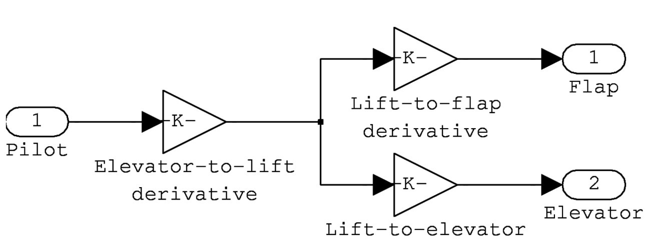

Fig. 17 Block diagram of the $\Delta C_p'$ maintenance function.

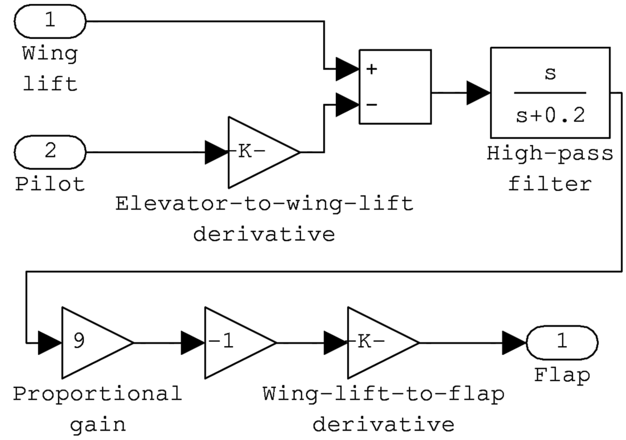

Fig. 18 Block diagram of the gust-alleviation function.

of interest is primarily 0.2 rad/s and above. The $\Delta C_p'$ optimization function uses a low-pass filter with a time constant of 20, and so its domain is primarily 0.05 rad/s and below. These two functions are unlikely to interfere with each other because their frequency domains do not intersect. The $\Delta C_p'$ maintenance function does not filter its input, and so all frequencies are in its domain. Its behavior must be examined with respect to each of the other functions.

The $\Delta C_p'$ optimization function attempts to drive $\Delta C_p'$ to the target value of -1.85. After it has been activated for some time, the value will either be very close to -1.85 (in smooth conditions) or varying around a mean close to -1.85 (in gusty conditions). If the pilot then requests a change in lift using the stick or yoke, the $\Delta C_p'$ maintenance function will use the flap and elevator to provide the requested change while maintaining the steady-state $\Delta C_p'$ of -1.85. Because both the optimization and maintenance functions are striving for the same $\Delta C_p'$ (-1.85), they complement each other and there is no interference.

The gust-alleviation function uses rapid flap motions to minimize deviations from the current wing lift coefficient. If the pilot requests a change in lift, the $\Delta C_p'$ maintenance function will attempt to provide this change, but the gust-alleviation function will quickly activate the flaps to prevent any change. These two functions will interfere with each other. This undesirable behavior would occur even if the $\Delta C_p'$ maintenance function were deactivated and the pilot directly controlled the elevator. Any attempt to change lift would be opposed by the gust-alleviation function.

For this reason, the gust-alleviation function must be modified slightly to take into account lift changes requested by the pilot. Figure 18 shows the complete model for the gust-alleviation function. Pilot input from the stick or yoke is multiplied by $(\mathrm{d}C_{L_w}/\mathrm{d}\delta_e)_{C_m=0}$ to determine the change in wing lift at the new trim condition for the requested elevator angle. This desired lift is subtracted from the actual wing lift to create a lift-coefficient error that is then sent to the high-pass filter. From this point on, the operation of the function is identical to that described previously.

Controller Performance

The three functions of the controller were tested separately and then together to assess their performance. To test the gust-alleviation function, a gust model was developed using uniform white noise with a sampling rate of 2 Hz. Note that this rate is not the rate at which the controller determines gusts by sampling pressures; this is the rate at which the current updraft/downdraft value changes in the simulation. In the simulation, the pressures are assumed to be sampled continuously. In planned future flight tests, the pressures will be sampled discretely but at some rate much higher than 2 Hz. Figure 19 shows the first 60 s of the vertical gust profile resulting from the model. The noise power was selected such that the size of an average gust is about 0.08 m/s, or about 1% of the aircraft speed. There is no horizontal (longitudinal or lateral) gust component.

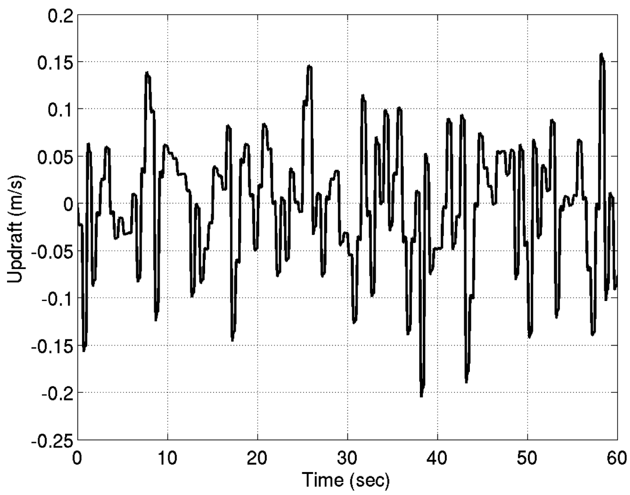

Fig. 19 Gust profile.

Figure 20 shows a 120 s simulation in which all controller functions are initially inactive, and the gust-alleviation function is activated at 60 s. Gust alleviation is effective in minimizing disturbances in both aircraft lift and the vertical acceleration felt at the aircraft center of gravity. Peak values for both parameters are reduced by about 65%. The tradeoff for this improvement is an increase in deviations about the mean $\Delta C_p'$. When a change in lift occurs due to a gust, the direction of flap motion required to alleviate it is opposite to the direction required to restore the previous $\Delta C_p'$, and so this increase in deviations is expected.

The gust-alleviation function requires rapid movement of the flap and precise knowledge of the instantaneous value of $\Delta C_p'$. In the simulation, simplifying assumptions are made for the flap servo and $\Delta C_p'$ determination. The flap servo is modeled as a continuous-time component (second-order filter), and $\Delta C_p'$ is determined using the instantaneous coefficient of lift provided by AeroSim Blockset. In a flight-test environment, R/C servo signals are typically generated 50 times per second, and this limits how quickly the servo can react. The measured value of $\Delta C_p'$ is also likely to be affected by unsteady aerodynamics and lag in the sensing system. Therefore, the gust-alleviation function may be difficult to implement and evaluate in a flight-test environment.

Figure 21 shows a simulation in which all controller functions are again initially inactive and the $\Delta C_p'$ optimization function is activated at 60 s. Over a period of about 10 s, the flap and elevator actuate to drive $\Delta C_p'$ from its starting value of about −2.04 toward the target value of −1.85. This is done without significant effects to the other aircraft parameters. This indicates that a slow-acting $\Delta C_p'$ optimization function could be added to an aircraft without causing undesirable changes to its dynamic response.

Figure 22 shows two responses to a request from the pilot for a −1 deg elevator change. In the uncontrolled case, the request (at 10 s) is passed directly to the elevator, and a classic phugoid response is observed. The value of $\Delta C_p'$ changes from −2.04 and oscillates around a mean of about −2.27. At 60 s, the $\Delta C_p'$ maintenance function is activated, and the next −1 deg request (at 70 s) is converted to a −0.2 deg elevator deflection and a +2.65 deg flap deflection. This combination results in the same phugoid response as the uncontrolled case, but the $\Delta C_p'$ oscillation is now about the original value and thus the steady-state $\Delta C_p'$ has not changed much. Because parameters other than $\Delta C_p'$ are virtually identical between the two cases, a fast-acting $\Delta C_p'$ maintenance function could also be added to an aircraft without undesirable dynamic response changes.

Figure 23 is similar to Fig. 22 except that both the $\Delta C_p'$ optimization and maintenance functions are activated at 60 s. Within about 10 s, $\Delta C_p'$ has moved from the initial value of −2.04 toward the target value of −1.85. When the pilot input is received at 70 s, $\Delta C_p'$ oscillates about the current (and target) value of −1.85. Other aircraft parameters show a phugoid response almost identical to the response

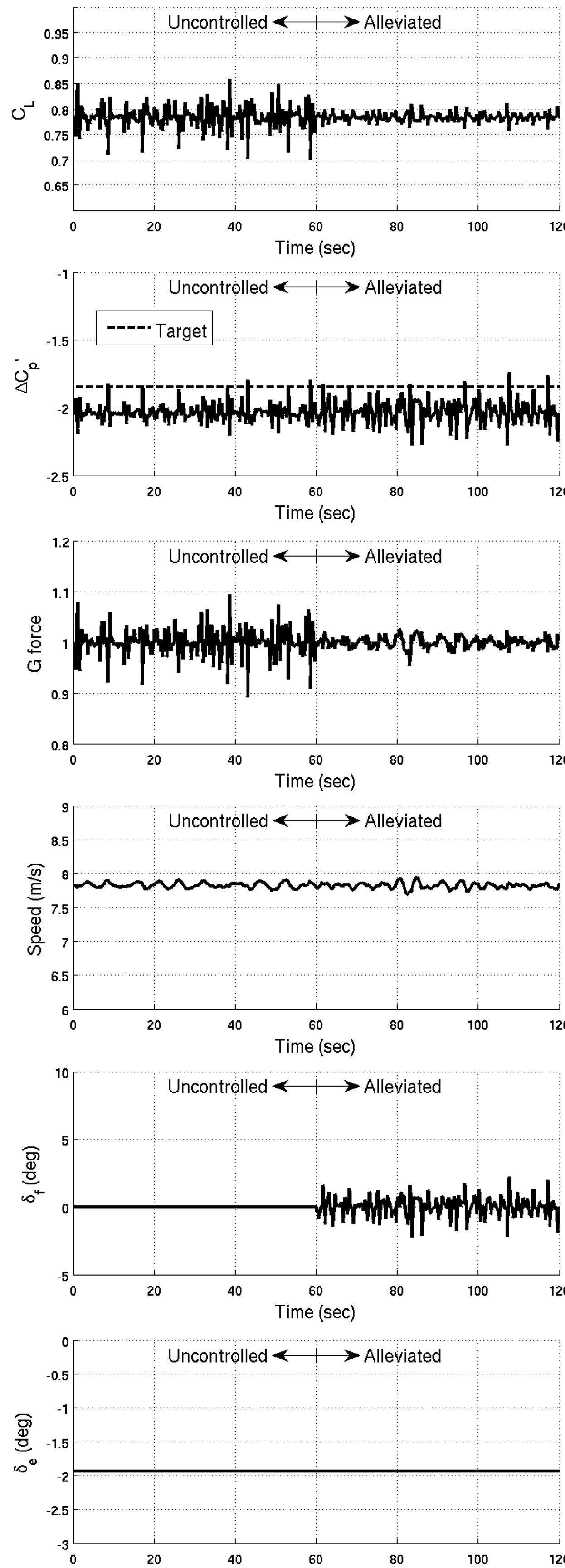

Fig. 20 Performance of the gust-alleviation function.

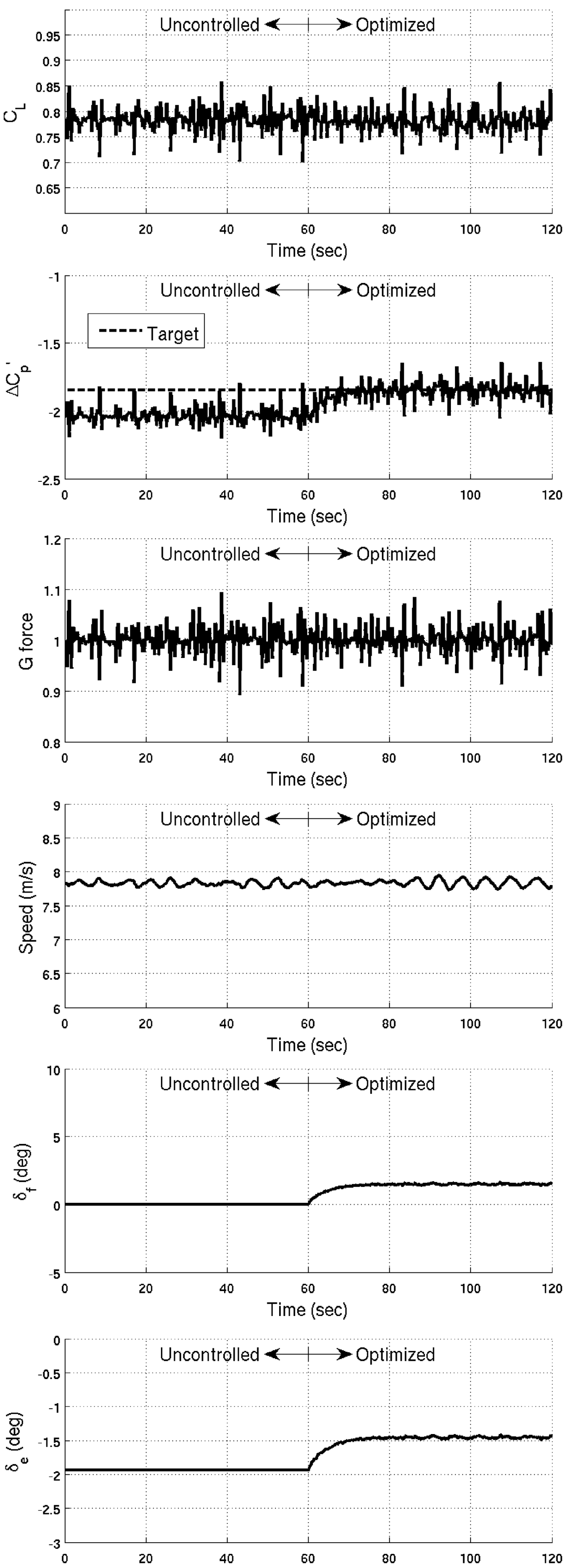

Fig. 21 Performance of the $\Delta C_p'$ optimization function.

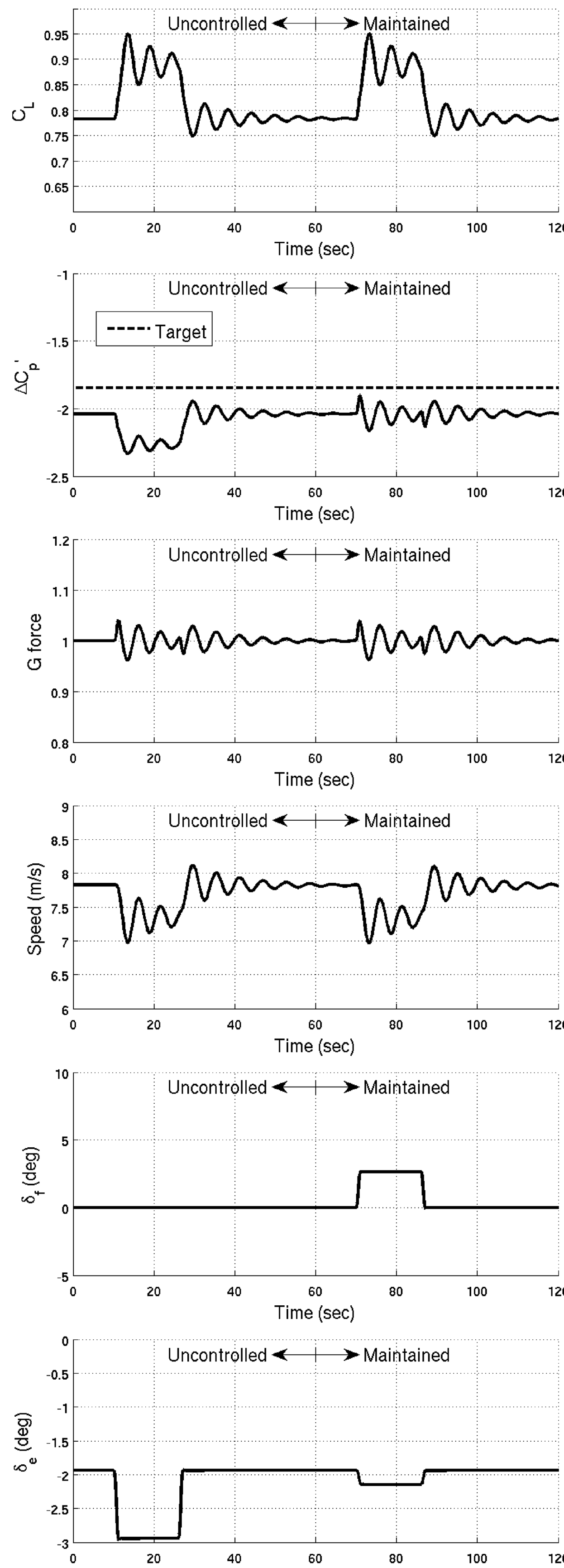

Fig. 22 Performance of the $\Delta C_p'$ maintenance function.

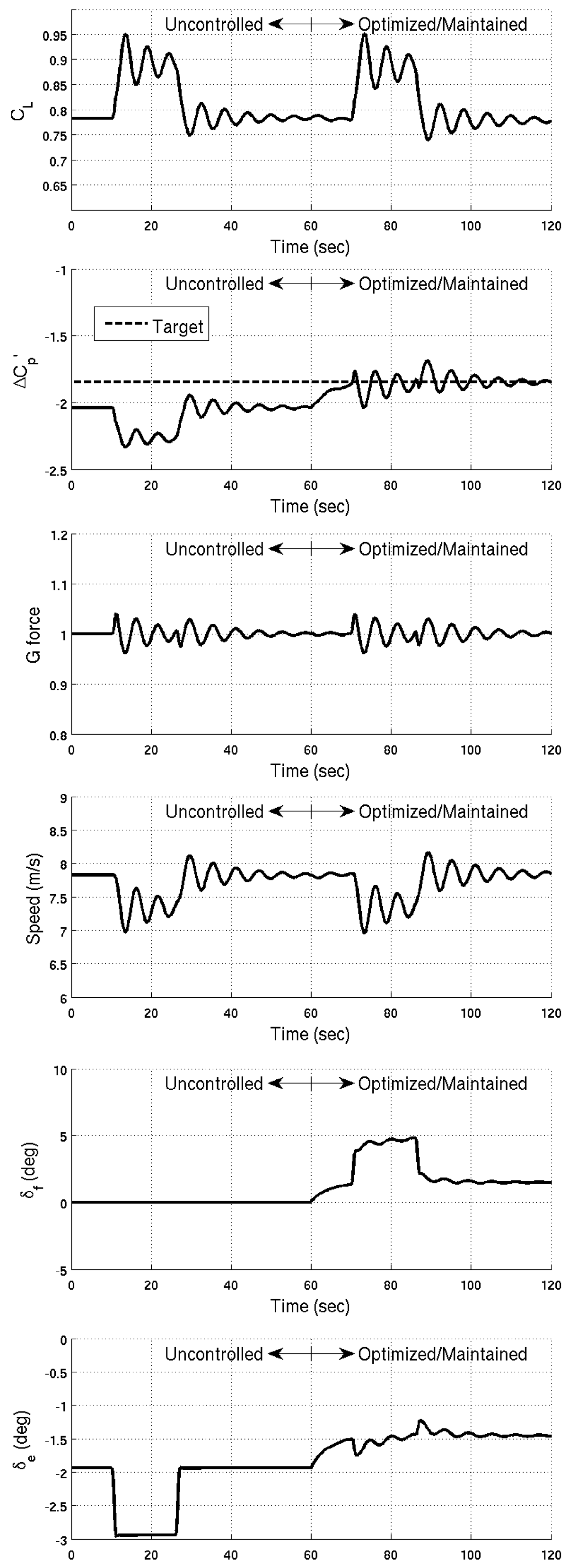

Fig. 23 Performance of the $\Delta C_p'$ optimization and maintenance functions.

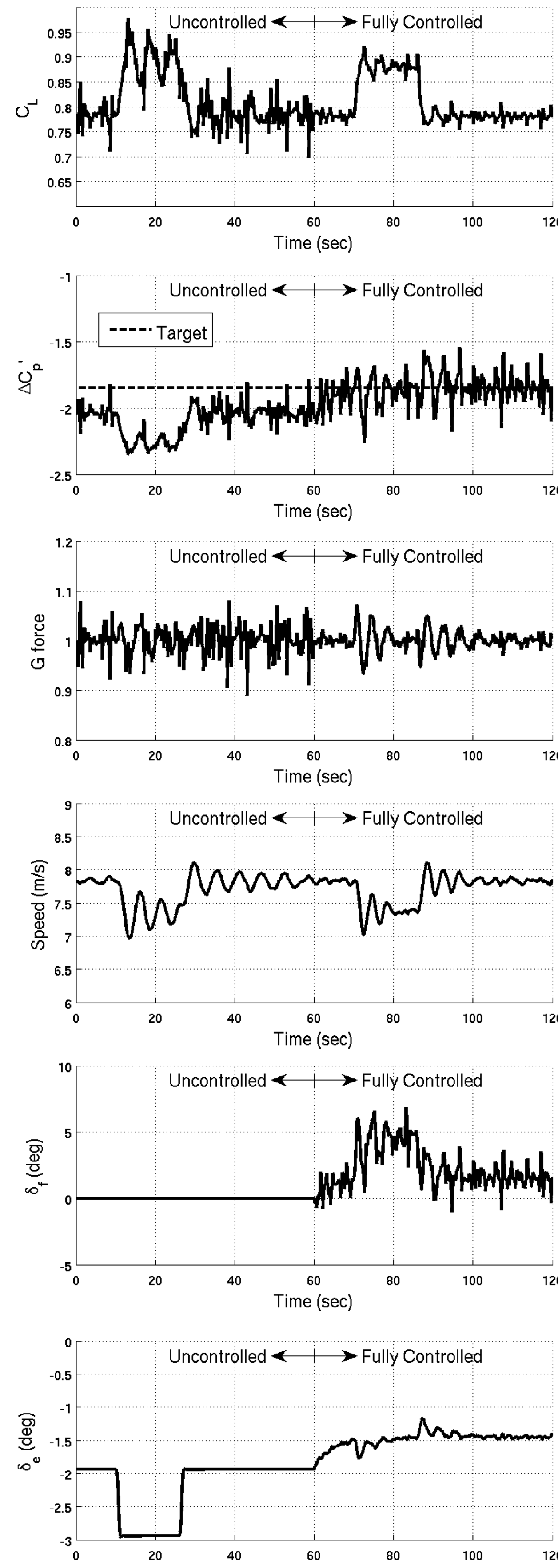

Fig. 24 Performance of the fully enabled controller.

of the uncontrolled (elevator only) aircraft. This indicates that a function implementing both slow-acting $\Delta C_p'$ optimization and fast-acting $\Delta C_p'$ maintenance could be added to an aircraft without adverse effects.

For the final simulation, all three controller functions (gust alleviation, $\Delta C_p'$ optimization, and $\Delta C_p'$ maintenance) are activated at 60 s. The inputs include the previously discussed gust profile and pilot requests from the stick or yoke. Figure 24 shows that gust alleviation is effective in reducing lift-coefficient perturbations (including phugoid oscillations) by about 65%. Reduction of vertical-acceleration perturbations averages about 40%, but it is dependent on pilot input. Perturbations immediately after a pilot input (at 70 and 85 s) are actually worse with the control functions activated than with the functions inactive (at 10 and 25 s). However, these increased vertical-acceleration perturbations occur only in response to aircraft stick or yoke movement, and so changes in vertical acceleration will be expected by the pilot. After the aircraft is able to settle into a steady-state condition (except for gusts), the controlled system has lower vertical-acceleration perturbations than the uncontrolled system. Airspeed perturbations are initially similar for both systems but appear to damp out quicker with the controller functions activated.

Conclusions

Simulations performed illustrate the effectiveness of using a three-function controller based on $\Delta C_p'$ data. Positive results were observed when the functions were tested separately, as well as when all functions were activated simultaneously. Gust alleviation was successful in reducing aircraft lift and vertical-acceleration perturbations in almost all instances. It also had the added effect of reducing phugoid oscillations. The $\Delta C_p'$ optimization was successful in maintaining a mean target $\Delta C_p'$ value, which reduced drag for the low Reynolds number SD7037 airfoil and should minimize drag for higher Reynolds number NLF airfoils. The $\Delta C_p'$ maintenance was successful in preventing large $\Delta C_p'$ changes due to pilot input. Although these changes would eventually be eliminated by the $\Delta C_p'$ optimization function, maintenance prevents them from occurring and thus allows mean $\Delta C_p'$ to remain constant even during response to pilot input.

Certain assumptions and simplifications were made in this research, and at least three improvements could be made to improve the current methodology.

1) Lifting surface models could be extended to incorporate the effects of unsteady aerodynamics associated with rapid flap motion.

2) The frequency response of the instrumentation system that determines $\Delta C_p'$ could be modeled.

3) Aeroelastic effects due to semisteady and unsteady forces could be included in the model.

Additionally, the effectiveness of the gust-alleviation controller depends on the availability of a flap actuator with an update rate significantly higher than the typical R/C rate of 50 Hz. However, the $\Delta C_p'$ optimization and $\Delta C_p'$ maintenance functions do not require special actuators and can be implemented with standard R/C servos. These two control functions can still be used without the gust-alleviation function on aircraft that do not have special low-latency flap actuators.

The performance seen in simulations of the three-function controller provides confidence to move to the flight-test portion of the research. In the near future, flight tests will be conducted with an instrumented Spirit 100 sailplane. One area of concern is the small leading-edge radius of the sailplane wing. This will make it difficult to ensure that the two leading-edge pressure ports necessary to calculate $\Delta C_p'$ are placed accurately. It is believed that in the future, this research can be conducted using full-scale experimental aircraft. The larger wing of such an aircraft will make it easier to ensure that the pressure ports necessary to determine $\Delta C_p'$ are placed accurately.

Acknowledgments

The authors would like to acknowledge KalScott Engineering for their partial support of this research through a Phase-2 Small Business Technology Transfer project from the NASA Dryden Research Center. Partial support for the first author was also provided by the Frank C. Ziglar Jr. Endowed Graduate Fellowship and is gratefully acknowledged.

References

[1] Pfenninger, W., "Investigation on Reductions of Friction on Wings, in Particular by Means of Boundary Layer Suction," NACA TM 1181, Aug. 1947.

[2] Pfenninger, W., "Experiments on a Laminar Suction Airfoil of 17 Per Cent Thickness," *Journal of the Aeronautical Sciences*, Vol. 16, No. 4, 1949, pp. 227–236.

[3] McGhee, R. J., Viken, J. K., Pfenninger, W., Beasley, W. D., and Harvey, W. D., "Experimental Results for a Flapped Natural-Laminar-Flow Airfoil with High Lift/Drag Ratio," NASA TM 85788, May 1984.

[4] Somers, D. M., "Design and Experimental Results for a Flapped Natural-Laminar-Flow Airfoil for General Aviation Applications," NASA TP 1865, June 1981.

[5] Drela, M., "Elements of Airfoil Design Methodology," *Applied Computational Aerodynamics*, edited by P. A. Henne, AIAA, Washington, D.C., Vol. 125, 1990, pp. 167–189.

[6] McAvoy, C., and Gopalarathnam, A., "Automated Cruise Flap for Airfoil Drag Reduction over a Large Lift Range," *Journal of Aircraft*, Vol. 39, No. 6, Nov.–Dec. 2002, pp. 981–988. doi:10.2514/2.3051

[7] Vosburg, V., and Gopalarathnam, A., "The Stability and Control of an Aircraft with an Adaptive Wing," AIAA Paper 2004-4814, Aug. 2004.

[8] Cox, C., Gopalarathnam, A., and Hall, C., "Analysis of Different Stabilizing Control Systems for Aircraft with Automated Cruise Flaps," AIAA Paper 2006-6134, Aug. 2006.

[9] AeroSim Blockset, Software Package, Ver. 1.2, Unmanned Dynamics, LLC, Hood River, OR, 2006.

[10] "Spirit 100 Instruction Book," Great Planes Model Manufacturing Co., Champaign, IL, 2005.

[11] Drela, M., and Youngren, H., *AVL 3.26 User Primer*, Dept. of Aeronautics and Astronautics, Massachusetts Inst. of Technology, Cambridge, MA, 2006.

[12] Selig, M. S., Donovan, J. F., and Fraser, D. B., *Airfoils at Low Speeds*, Soartech No. 8, SoarTech Publications, Virginia Beach, VA, 1989.

[13] Drela, M., "XFOIL: An Analysis and Design System for Low Reynolds Number Airfoils," *Low Reynolds Number Aerodynamics*, edited by T. J. Mueller, Lecture Notes in Engineering, Vol. 54, Springer–Verlag, New York, 1989, pp. 1–12.